

LASER INTERFEROMETER GRAVITATIONAL WAVE OBSERVATORY  
- LIGO -  
CALIFORNIA INSTITUTE OF TECHNOLOGY  
MASSACHUSETTS INSTITUTE OF TECHNOLOGY

Technical Note	LIGO-T2100239-	2021/09/01
<b>Low-noise Nonlinear Cavity for Cryogenic Interferometers</b>		
R. Youssef, R.X Adhikari, A. Gupta, F. Salces-Carcoba		

**California Institute of Technology**  
**LIGO Project, MS 18-34**  
**Pasadena, CA 91125**  
Phone (626) 395-2129  
Fax (626) 304-9834  
E-mail: info@ligo.caltech.edu

**Massachusetts Institute of Technology**  
**LIGO Project, Room NW22-295**  
**Cambridge, MA 02139**  
Phone (617) 253-4824  
Fax (617) 253-7014  
E-mail: info@ligo.mit.edu

**LIGO Hanford Observatory**  
**Route 10, Mile Marker 2**  
**Richland, WA 99352**  
Phone (509) 372-8106  
Fax (509) 372-8137  
E-mail: info@ligo.caltech.edu

**LIGO Livingston Observatory**  
**19100 LIGO Lane**  
**Livingston, LA 70754**  
Phone (225) 686-3100  
Fax (225) 686-7189  
E-mail: info@ligo.caltech.edu

# Contents

<b>1</b>	<b>Introduction</b>	<b>2</b>
<b>2</b>	<b>Background</b>	<b>2</b>
<b>3</b>	<b>Experimental Setup</b>	<b>3</b>
3.1	The DOPO Setup . . . . .	3
3.2	Noise Detection . . . . .	4
<b>4</b>	<b>Noise Calculations</b>	<b>5</b>
4.1	Mirrors 1 and 2 . . . . .	6
4.2	Seismic Noise . . . . .	7
4.3	Free-running frequency noise . . . . .	7
4.4	Total Noise . . . . .	7
<b>5</b>	<b>Temperature Tuning Curve</b>	<b>8</b>
5.1	Derivation . . . . .	8
5.2	Tuning Curve Plot . . . . .	10
<b>6</b>	<b>Conclusion</b>	<b>10</b>

## 1 Introduction

First detected by LIGO [1], gravitational waves (GW) offered valuable insights into astronomical phenomena that are crucial to our understanding of the universe. At its core, LIGO is modeled after the famous Michelson interferometer with arms of 4 kilometers and suspended mirrors to reflect a powerful laser beam. The passage of GW introduces changes in the arm length on the order of  $10^{-21}$  meter. By analyzing the interference pattern taking place at the photodetector, the change in arm length due to GW can be detected. Due to the sensitive nature of its measurements, LIGO continually seeks to improve its sensitivity. Currently, scientists are aiming for a 100-times better sensitivity than the first-generation instruments [2]. Achieving this improvement requires keeping the test masses at 123 K as well as changing the material that the mirrors are made of [3]. The new material, crystalline silicon, absorbs the wavelength of the existing laser. Therefore, the change of the test masses material will necessitate a change in the laser's frequency from 1064 nm to 2128 nm, which will not be heavily absorbed by the new test masses. The change of wavelength is achieved through a Degenerate Optical Parametric Oscillator (DOPO). Due to many noise sources, the wavelength conversion process may not be perfect. In this project, we are investigating and quantifying the sources of frequency noise in DOPO as well as methods to detect it and mitigate it if necessary.

## 2 Background

A DOPO is a device that is used to generate electromagnetic waves of desired frequencies through nonlinear processes. Typically, there is an intense laser source that is pumped through a nonlinear crystal, Potassium Titanyl Phosphate (PPKTP), which in turn converts the pumped frequency to the desired value. As shown in Fig. 1(b), a laser beam of frequency  $\omega_p$  is pumped into an optical cavity that contains a dielectric non-linear medium of second-order susceptibility,  $\chi^{(2)}$ . Through the non-linear processes that take place inside the crystal, photons of new frequency are generated:  $\omega_s$  (signal frequency) and  $\omega_I$  (idler frequency). In our case, this is a degenerate OPO, so  $\omega_I = \omega_s = \omega$ , as shown in Fig. 1(b). For optimum nonlinear frequency conversion, the phase mismatch value  $\Delta k = k_3 - k_2 - k_1$  needs to be as close as possible to zero. To fulfill the  $\Delta k = 0$  condition, a periodically-poled crystal is used to ensure that the field strength of the generated wave grows linearly with the propagation distance [4]. On a microscopic level, the frequency conversion process is parametric, meaning that the initial and final quantum-mechanical states of the system are identical. In effect, the ground state population is only temporarily removed for brief intervals of time to reside in virtual levels, as shown in Fig. 1(a) [4].

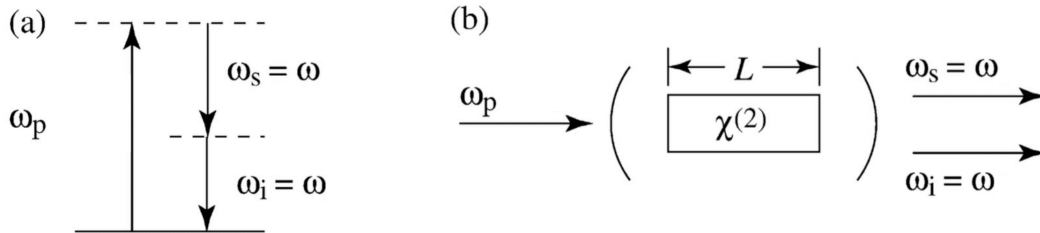


Figure 1: (a) A microscopic view of the processes inside the nonlinear medium. The dashed lines represent virtual energy levels, whereas the solid line represents the ground state. (b) The experimental setup of an Optical Parametric Oscillator. The curved lines surrounding the non-linear crystal represent mirrors that reflect waves with frequency  $\omega$ . [4]

## 3 Experimental Setup

### 3.1 The DOPO Setup

DOPO is currently set up in the lab on an optical table, as shown in Fig. 2. The goal of the optical cavity is to amplify the intensity of the laser beam after converting its wavelength to 2128 nm. In this setup, a 1064 nm laser beam with approximately 34  $\mu\text{m}$  beam waist is fed to the optical cavity. The input coupler is a highly reflective mirror with a 15 mm radius of curvature and plano concave 7979 infrasil substrate with 99.95% high reflectivity coating at both 1064 nm and 2128 nm. The high reflectivity of the input coupler prevents the amplified beam from being reflected back to the laser. The output coupler is also a mirror with a 25 mm radius of curvature and plano concave 7979 infrasil substrate with 99.95% high reflectivity coating at 1064 nm but 97% at 2128 nm. That way, there is a high probability for 2128 nm photons to be transmitted through the output coupler.

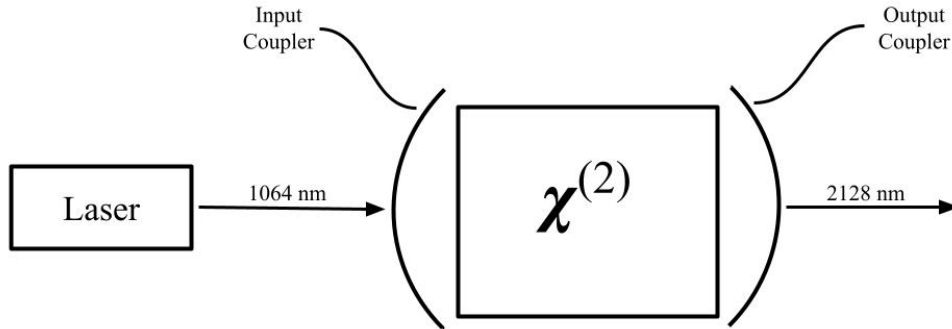


Figure 2: The setup of DOPO that is mounted on an optical table. The distance between the input and output couplers is 47.5 nm.

### 3.2 Noise Detection

The end goal of this project is to measure the frequency noise of DOPO. There are two possible schemes to measure the frequency noise: heterodyne and homodyne. In our case, we chose a heterodyne scheme as it operates in the terahertz range, making the signal less susceptible to ambient low-frequency noise. The low-frequency noise is typically introduced by many environmental sources such as seismic noise. Since the experiment is not set up in a seismically-isolated vacuum chamber, many types of low-frequency noise will not be eliminated. Hence, it is necessary to have a detection scheme that operates in a frequency band that is higher than environmental noise. That way, the signal has high frequency and the surrounding environment noise has small impact on the signal.

Heterodyne detection measures the phase difference between two arms by interpreting their interference pattern. As shown in Fig. 3, a heterodyne scheme requires a local oscillator that introduces frequency shift (usually on the order of Megahertz) to one of the arms through the acoustic-optic modulator (AOM). After the laser beam is passed through the AOM, the new beam's frequency will be the sum of the laser frequency and AOM's local oscillator's frequency ( $\omega_L + \omega_A$ ). When the two arms combine in the second beam splitter (BS 2), the intensity of the new beam is a function of the phase difference between the two arms. Thus, measuring the light intensity of the combined beam will allow us to calculate the phase

difference between the two arms. Specifically, the photodetector's intensity is given by

$$I_{detected} = I_0 \left[ 1 + \cos \left( (\omega_A - \omega_D - \omega_s)t \right) \right] \quad (1)$$

where  $\omega_A$  is the frequency introduced by AOM,  $\omega_D$  is the frequency introduced by DOPO, and  $\omega_s$  is the frequency introduced by SHG. The intensity,  $I$ , for a heterodyne scheme is time-dependant. It also depends on the phase difference between the first arm ( $\omega_A$ ) and the second arm ( $\omega_D + \omega_s$ ).

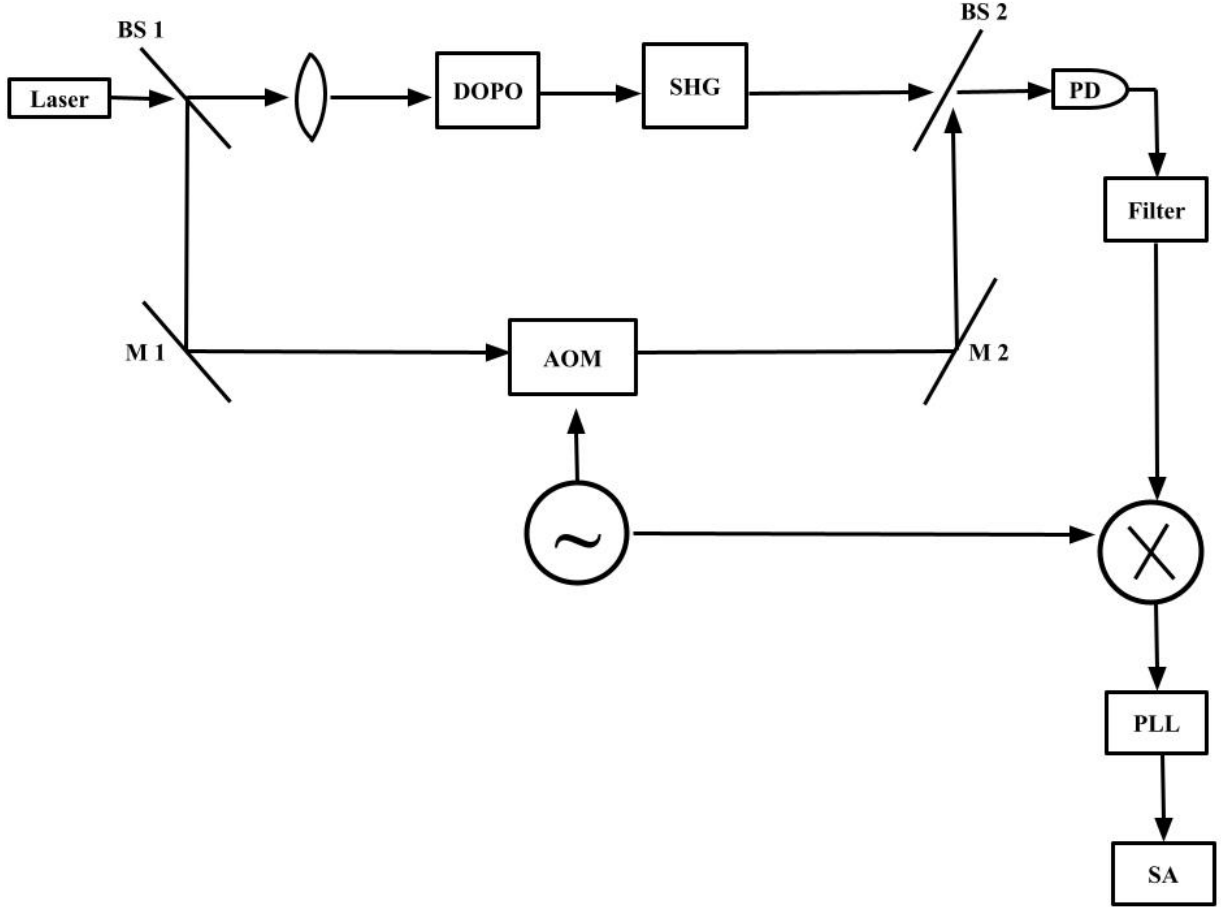


Figure 3: Heterodyne detection scheme to measure the frequency noise of DOPO. The first arm is the one including DOPO and SHG, whereas the second arm is the one including AOM. The mirrors, M1 and M2, are highly reflective. The angular frequency  $\omega_L, \omega_D, \omega_S$  and  $\omega_A$  represent laser frequency, DOPO's frequency, SHG's frequency, and AOM's frequency, respectively.

## 4 Noise Calculations

There are many ways to classify noise sources in a given experiment. Here, we classified noise by electronic components or optical setups that produce them. In our analysis, we

need to make sure that the power spectral density functions are valid in the 5 Hz - 5 KHz range because this is the range in which LIGO operates. Some of the noise sources that we plotted are shown below

#### 4.1 Mirrors 1 and 2

The substrate of these mirrors is fused silica and the coating is made of fused silica ( $SiO_2$ ) and tantala ( $Ta_2O_5$ ). The mirror are round with a diameter of 1 inch, so the area is  $\pi r^2 = \pi(0.0127)^2$ . The thickness of the substrate is 0.005 m and the coating is  $4.72\mu m = 4.72 \times 10^{-6}$  m (2.75 $\mu$  m of silica + 1.97 $\mu$ m of tantala). There are many forms of thermal noise in these mirrors. So far, we considered some types of thermal noise in the substrate of the mirrors. Specifically, we considered the thermo-refractive and thermo-optic noise.

- **Thermo-refractive Noise:** describes how temperature fluctuations induced by the laser change the refractive index of the mirrors' coating, which in turn changes the resonant frequency of the mirrors.

$$S(f) = \frac{4a\beta^2}{\pi^3 w^4 f^2} \frac{\kappa k_B T^2}{\rho^2 C^2} \quad (2)$$

where  $w$  is the radius of the Gaussian beam,  $a$  is the thickness of the plate,  $\rho$  is the density of the substrate,  $C$  is the specific heat capacity, and  $\kappa$  is the thermal conductivity. [3].

- **Thermo-optic noise** represents the coherent sum of thermo-elastic and thermo-refractive noise. The coherent sum of the power spectrum of both sources of noise is given by

$$S_{TO}^{\Delta z} \simeq S_{TO}^{\Delta T} \left( \bar{\alpha}_c d - \bar{\beta} \lambda - \bar{\alpha}_s d \frac{C_c}{C_s} \right)^2 \quad (3)$$

where

$$S_{TO}^{\Delta T} = \frac{2\sqrt{2}}{\pi} \frac{k_B T^2}{r_G^2 \sqrt{\kappa C \omega}}$$

where  $\kappa$  is the thermal conductivity of substrate,  $r_G^2$  is the beam radius, and  $C$  is the heat capacity per volume. Additionally,  $\bar{\alpha}_c$  is the effective coefficient of thermal expansion of the coating,  $\bar{\beta}$  is the the effective thermo-refractive coefficient,  $d$  is the coating thickness, and  $C_s$  and  $C_c$  represent the heat capacity per volume of the substrate and coating respectively [5].

As shown in Figure 4, the thermo-refractive and thermo-optic noise introduced by the substrate of M1 and M2 are extremely small.

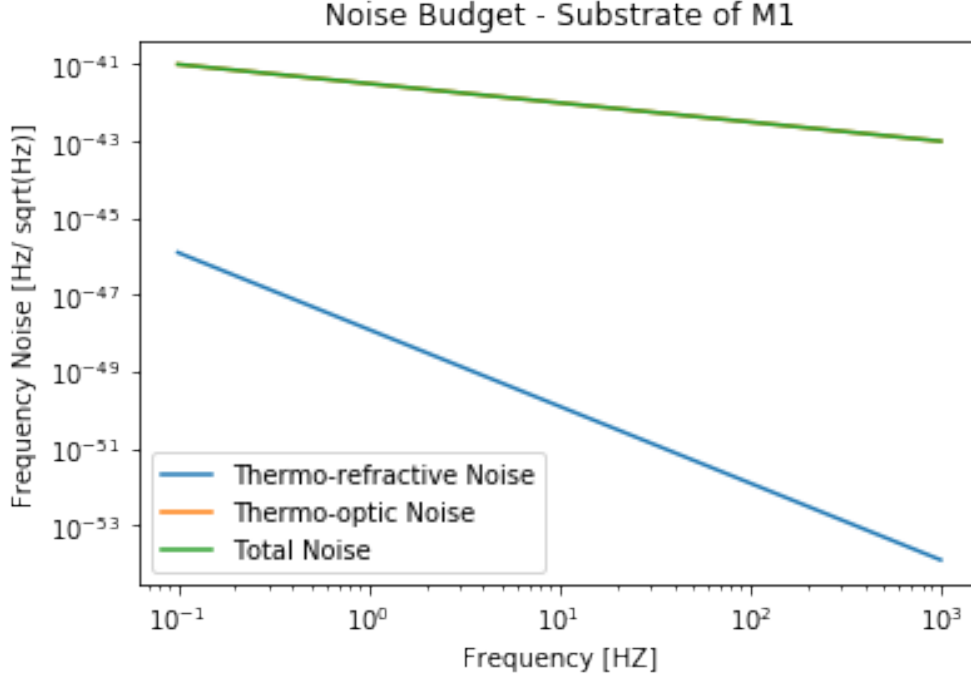


Figure 4: Noise Budget for the substrate of mirror 1. The noise introduced by mirror 2 will be identical to mirror 1.

## 4.2 Seismic Noise

The optical table's transfer function suppresses seismic noise in the 1 - 100 Hz band. Its transfer function is proportional to

$$S(f) = \frac{1}{f^2} \quad (4)$$

## 4.3 Free-running frequency noise

The laser used to pump DOPO utilizes a non-planar ring oscillator (NPRO). The frequency noise associated with this laser is given by

$$S(f) = \frac{10^4}{f} \quad (5)$$

## 4.4 Total Noise

When these noise contributions (subsection 4.1 – 4.4) are compared, it is evident that the noise introduced by the substrate is several orders of magnitude smaller than other sources (i.e. laser and seismic noise), as shown in Fig. 5. Furthermore, the laser beam bounces once off of mirrors 1 and 2, meaning that the losses caused by these mirrors are not significant. On the other hand, it bounces a lot more inside the cavity, so we should be more concerned with the noise inside the cavity. For these two reasons, the frequency noise introduced by these mirrors can be neglected in our analysis.

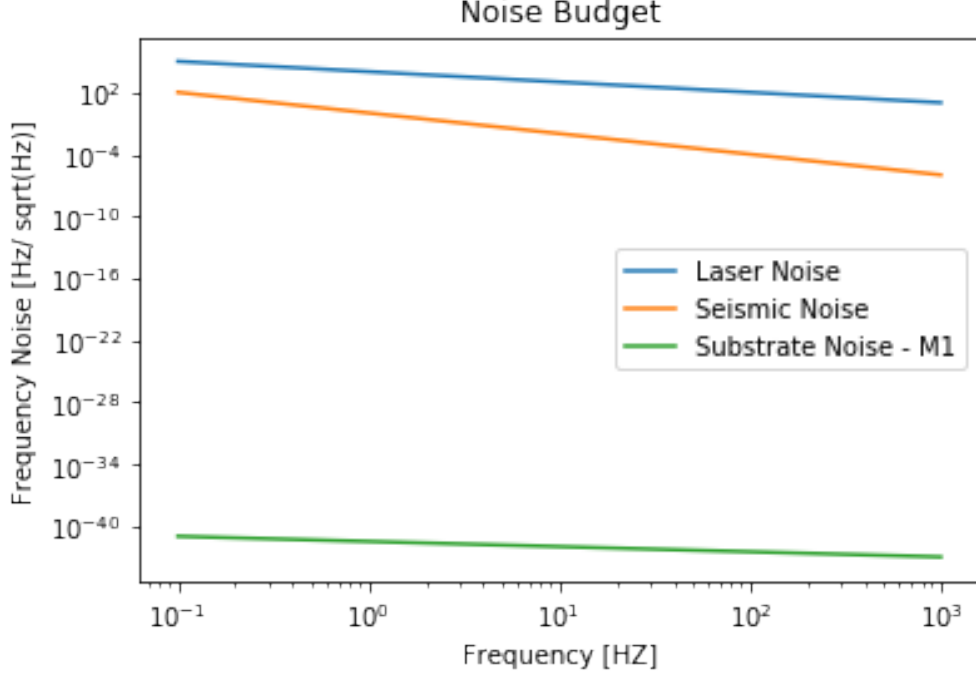


Figure 5: Noise budget of frequency noise sources that exist in a heterodyne detection scheme.

## 5 Temperature Tuning Curve

### 5.1 Derivation

Since this is a degenerate down parametric conversion, we know that

$$\omega_1 = \omega_2 + \omega_3 \quad (6)$$

where  $\omega_1$  is the pump frequency of the laser ( $\lambda_p = 1064$  nm), and  $\omega_2$  and  $\omega_3$  represent idler and signal frequency. Since this is a degenerate process,  $\omega_2 = \omega_3$

From the wave vector mismatch condition, we find that

$$\Delta k = k_1 - k_2 - k_3 - \frac{2\pi}{\Lambda(T)} \quad (7)$$

where  $\Lambda(T) = \Lambda_0(1 + \alpha\Delta T)$  is the poling period of the PPKTP crystal, and  $\Lambda_0 = 38.85 \times 10^{-6}$  m,  $\alpha = 5 \times 10^{-6}$  is the thermal expansion coefficient. Ideally, we want  $\Delta k = 0$ .

Near the degeneracy point,  $T_0$ , we can assume that  $\omega_2 = \frac{\omega_1}{2} + \Delta\omega$  and  $\omega_3 = \frac{\omega_1}{2} - \Delta\omega$ , so we get

$$0 = k(\omega_1) - k\left(\frac{\omega_1}{2} + \Delta\omega\right) - k\left(\frac{\omega_1}{2} - \Delta\omega\right) - \frac{2\pi}{\Lambda(T)}$$

We can Taylor expand around  $\frac{\omega_1}{2}$  to get

$$0 = k(\omega_1) - k\left(\frac{\omega_1}{2}\right) - k'\left(\frac{\omega_1}{2}\right) + \frac{1}{2}k''\left(\frac{\omega_1}{2}\right)\Delta\omega^2 - k\left(\frac{\omega_1}{2}\right) + k'\left(\frac{\omega_1}{2}\right) + \frac{1}{2}k''\left(\frac{\omega_1}{2}\right)\Delta\omega^2 - \frac{2\pi}{\Lambda(T)}$$

Note that  $k'\left(\frac{\omega_1}{2}\right) < 0$  and  $k''\left(\frac{\omega_1}{2}\right) < 0$  for the PPKTP crystal.

$$0 = k(\omega_1) - 2k\left(\frac{\omega_1}{2}\right) + k''\left(\frac{\omega_1}{2}\right)\Delta\omega^2 - \frac{2\pi}{\Lambda(T)}$$

Let  $\beta = k''\left(\frac{\omega_1}{2}\right)$  be the anomalous dispersion coefficient, so the equation becomes

$$0 = k(\omega_1) - 2k\left(\frac{\omega_1}{2}\right) + \beta\Delta\omega^2 - \frac{2\pi}{\Lambda(T)}$$

Now plug the values to have

$$0 = \frac{n_1\omega_1}{c} - \frac{2n_2\omega_1}{2c} + \beta\Delta\omega^2 - \frac{2\pi}{\Lambda_0(1 + \alpha\Delta T)}$$

Finally, solving for  $\Delta\omega$  yields

$$\Delta\omega = \pm \sqrt{\frac{2\pi}{\beta\Lambda_0(1 + \alpha\Delta T)} - \frac{\omega_1(n_1 - n_2)}{\beta c}}$$

It then follows that

$$\omega_{2,3} = \frac{\omega_1}{2} \pm \sqrt{\frac{2\pi}{\beta\Lambda_0(1 + \alpha\Delta T)} - \frac{\omega_1(n_1 - n_2)}{\beta c}} \quad (8)$$

From dimensional analysis, we find that  $[\beta] = \frac{s^2}{m}$ , which represents the group velocity dispersion. Furthermore, we know that  $n_1$  and  $n_2$  depend on wavelength and temperature according to this equation

$$n_{1,2} = n_z + \Delta n$$

where

$$n_{1,2} = \sqrt{4.59432 + \frac{0.06206}{\lambda_n^2 - 0.04763} + \frac{110.80672}{\lambda_n^2 - 0.04763} + 3.98 \times 10^{-5} + x_1(\lambda)(T-300) + x_2(T-300)^2} \quad (9)$$

where

$$x_{1,2}(\lambda) = \sum_{m=0}^3 \frac{a_m}{\lambda^m}$$

The value of  $n_z$  is given by Sellmeier equation [9] where the constants are measured experimentally. Also, the values of  $a_m$  are determined experimentally [10]. From equation 8, we clearly see that DOPO's efficiency can be controlled through its temperature. The temperature oven available in the lab now is accurate to 0.1 C°.

## 5.2 Tuning Curve Plot

Using Equation 9, we obtain the following curve

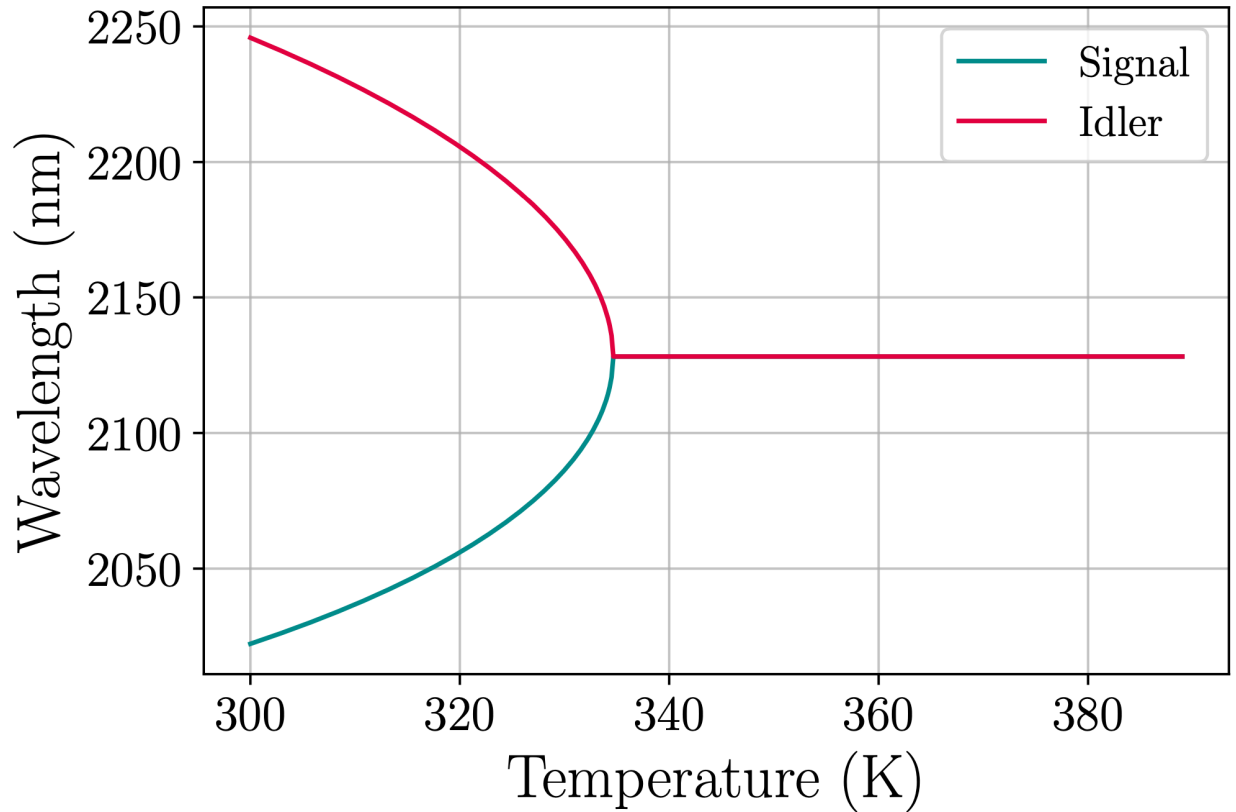


Figure 6: Temperature tuning curve of DOPO.

From this plot, we see that DOPO's optimal temperature happens around 335 K. At this optimal temperature, the photons produced by DOPO will have the desired wavelength, 2128 nm. Since the temperature oven is accurate to 0.1 C°, DOPO needs to be operated at a temperature slightly higher than the optimal temperature. If operated exactly at the optimal temperature, temperature fluctuations from the oven can reduce its efficiency.

## 6 Conclusion

From this project, there are a few conclusions that can be made. First, a heterodyne detection scheme works better for our purposes. Given that this is a table-top experiment, there will be low-frequency noise sources from the surrounding environment whose impact can only be mitigated through a heterodyne scheme. Second, the noise introduced by mirrors 1 and 2 are negligible compared to other electronic components from the measurement scheme. Hence, thermal noise from these two mirrors can be omitted from the analysis needed to measure DOPO's noise. Finally, the temperature oven of DOPO needs to be operated at a slightly higher temperature ( $> 0.1$  C°) than the optimal temperature, hence, the price to pay is a drop in conversion efficiency.

## References

- [1] R. Abbott et al 2021 ApJL 915 L5.
- [2] Hild, Stefan. (June 2010). Concepts for third generation Gravitational Wave detectors. LISA Symposium, Stanford. <https://dcc.ligo.org/LIGO-G1000659/public>.
- [3] R X Adhikari et al 2020 Class. Quantum Grav. 37 165003.
- [4] Boyd, Robert W. (April 11, 2008). Nonlinear Optics. Academic Press.
- [5] Evans, M., Ballmer, S., Fejer, M., Fritschel, P., Harry, G., amp; Ogin, G. (2008). Thermo-optic noise in coated mirrors for high-precision optical measurements. *Physical Review D*, 78 (10). <https://doi.org/10.1103/physrevd.78.102003>.
- [6] “Gaussian Beam PROPAGATION: *Edmund Optics*.” Edmund Optics Worldwide, [www.edmundoptics.com/knowledge-center/application-notes/lasers/gaussian-beam-propagation/](http://www.edmundoptics.com/knowledge-center/application-notes/lasers/gaussian-beam-propagation/).
- [7] Crystran. ”Silica Glass ( $\text{SiO}_2$ )”. *Silica Glass ( $\text{SiO}_2$ ) Optical Material*. <https://www.crystran.co.uk/optical-materials/silica-glass-sio2>
- [8] The LIGO Scientific Collaboration et al 2015 Class. Quantum Grav. 32 074001
- [9] Aerie. Ady et al. “Temperature-dependant Dispersion Equations for  $\text{KTiOPO}_4$  and  $\text{KTiOASO}_4$ ”. December 2003.
- [10] Kato, Kiyoshi et al. “Sellmeier and thermo-optic dispersion formulas for KTP”. 2002.